Extremophiles (2014) 18:545–560
DOI 10.1007/s00792-014-0640-2

ORIGINAL PAPER

Biosignatures in chimney structures and sediment from the Loki's Castle low-temperature hydrothermal vent field at the Arctic Mid-Ocean Ridge

Andrea Jaeschke · Benjamin Eickmann · Susan Q. Lang · Stefano M. Bernasconi · Harald Strauss · Gretchen L. Früh-Green

Received: 19 September 2013 / Accepted: 2 March 2014 / Published online: 23 March 2014

Abstract We investigated microbial life preserved in a hydrothermally inactive silica–barite chimney in comparison with an active barite chimney and sediment from the Loki's Castle low-temperature venting area at the Arctic Mid-Ocean Ridge (AMOR) using lipid biomarkers. Carbon and sulfur isotopes were used to constrain possible metabolic pathways. Multiple sulfur ($\delta^{34}S$, $\Delta^{33}S$) isotopes on barite over a cross section of the extinct chimney range between 21.1 and 22.5 ‰ in $\delta^{34}S$, and between 0.020 and 0.034 ‰ in $\Delta^{33}S$, indicating direct precipitation from seawater. Biomarker distributions within two discrete zones of this silica–barite chimney indicate a considerable difference in abundance and diversity of microorganisms from the chimney exterior to the interior. Lipids in the active and inactive chimney barite and sediment were dominated by a range of ^{13}C-depleted unsaturated and branched fatty acids with $\delta^{13}C$ values between −39.7 and −26.7 ‰, indicating the presence of sulfur-oxidizing and sulfate-reducing bacteria. The majority of lipids (99.5 %) in the extinct chimney interior that experienced high temperatures were of archaeal origin. Unusual glycerol monoalkyl glycerol tetraethers (GMGT) with 0–4 rings were the dominant compounds suggesting the presence of mainly (hyper-) thermophilic archaea. Isoprenoid hydrocarbons with $\delta^{13}C$ values as low as −46 ‰ also indicated the presence of methanogens and possibly methanotrophs.

Keywords Hydrothermal · Silica chimney · Barite · Biomarker · GDGT · GMGT · Multiple S isotopes

Introduction

The capacity to survive under extreme conditions is a fundamental requirement for life at deep-sea hydrothermal

Communicated by A. Oren.

A. Jaeschke (✉) · S. Q. Lang · G. L. Früh-Green
Department of Earth Sciences, Institute of Geochemistry and Petrology, ETH Zurich, Clausiusstrasse 25, 8092 Zurich, Switzerland
e-mail: andrea.jaeschke@awi.de

Present Address:
A. Jaeschke
Alfred Wegener Institute for Polar- and Marine Research, Am Alten Hafen 26, 27568 Bremerhaven, Germany

B. Eickmann
Department of Earth Science, Centre for Geobiology, University of Bergen, Allegaten 41, 5007 Bergen, Norway

Present Address:
B. Eickmann
Department of Geology, University of Johannesburg, Auckland Park, Johannesburg 2006, South Africa

Present Address:
S. Q. Lang
Department of Earth and Ocean Sciences, University of South Carolina, Columbia, SC 29208, USA

S. M. Bernasconi
Department of Earth Sciences, Geological Institute, ETH Zurich, Sonneggstrasse 5, 8092 Zurich, Switzerland

H. Strauss
Institut für Geologie und Paläontologie, Westfälische Wilhelms-Universität Münster, Corrensstr. 24, 48149 Münster, Germany

vents (Kelly et al. 2002). These specific environments provide microhabitats for a diversity of heat-adapted prokaryotes gaining energy by the oxidation and reduction of inorganic compounds like elemental sulfur, hydrogen, nitrate, various metal oxides and sulfides (Amend and Shock 2001; Miroshnichenko 2004; Schönheit and Schäfer 1995). The extreme thermophilic chemolithoautotrophs that are deeply rooted within the universal phylogenetic tree are the main primary producers, thus being fundamental for all other organisms inhabiting deep-sea vent ecosystems (Reysenbach and Cady 2001). The most critical metabolic requirement at very high temperatures is the maintenance of functional lipid membranes. Especially within the archaea, there are members having the highest growth temperatures known to date at 121 °C (Kashefi and Lovley 2003). This resilience may be partly due to their unique membrane lipids composed of glycerol dialkyl glycerol tetraethers (GDGTs). GDGTs are membrane-spanning lipids composed of isoprenoid chains linked to a glycerol backbone by ether bonds, resulting in higher rigidity and sustaining membrane fluidity also at high temperatures, pressures, heavy metal contents or low pH (Boyd et al. 2011). Therefore, archaeal lipids may be better suited to extreme environments than the ester-type bilayer lipids of bacteria or eukarya (Van de Vossenberg et al. 1998). Since the discovery of the first deep-sea hydrothermal vents about 30 years ago (Corliss et al. 1979), many more active sites have been discovered on modern spreading centers mainly on mid-ocean ridges and in back-arc basins. They are typically associated with polymetallic massive sulfide deposits formed by the mixing of hot anoxic vent fluid and cold oxic seawater (Herzig and Hannington 1995; Tivey 1995). Diffuse venting occurs at the margins of existing high-temperature upflow, and minerals precipitated at low temperatures (generally <10–50 °C) typically consist of amorphous Fe–Mn oxides, barite, and silica (Herzig and Hannington 1995). The massive chimney structures of both high- and low-temperature vents harbor diverse microbial communities ranging from mesophiles to hyperthermophiles. However, vent chimneys finally become hydrothermally inactive leading to a drastic change in community structure as a result of extinct energy sources (Suzuki et al. 2004; Kato et al. 2010). The diversity and abundance of microbial communities in active vent structures have been reported using culture-independent approaches (Kormas et al. 2006; Schrenk et al. 2003; Takai et al. 2001). Our knowledge about microbial communities in inactive chimneys or even past traits of microbial life is still fragmentary (Kato et al. 2010; Suzuki et al. 2004). Organic geochemistry offers a complementary view on active and fossil microbial communities. However, biomarker studies on modern or ancient hydrothermal vent systems are still sparse (Blumenberg et al. 2007, 2012; Gibson et al. 2013; Jaeschke et al. 2012; Lincoln et al. 2013). Our current knowledge is mainly based on lipid analysis of isolated and enriched microorganisms, while it is unclear how their activity compares to those of complex natural communities. Moreover, the preservation potential of specific biomarker lipids in the geological record is as yet unknown (Blumenberg et al. 2012). Our study aims at getting insights into microbial life preserved in an extinct silica–barite chimney of unknown age as well as in an actively venting barite chimney and sediment from a low-temperature diffuse venting area discovered in close vicinity to Loki's Castle main black smoker vent field at the Arctic Mid-Ocean Ridge (AMOR), using a combination of organic and inorganic geochemical methods.

Materials and methods

Study area and sampling

Loki's Castle is a deep-sea hydrothermal vent field that was discovered in 2008 at the AMOR at 73°30′N and 8°E (Fig. 1) (Pedersen et al. 2010). It is located at 2400 m depth on an axial volcanic ridge at the southern end of the Knipovich Ridge, which is one of the slowest spreading ridge segments on Earth ($\sim$6 mm a^{-1}). The main vent field is composed of four active black smoker chimneys distributed on two mounds of hydrothermal sulfide deposits that are around 150 m apart. The vent fluids with temperatures of 310–320 °C and pH of 5.5 are characterized by high concentrations of methane, hydrogen, and ammonia, indicating a sediment-influenced hydrothermal vent system (Lilley et al. 1993). A low-temperature diffuse venting area located at the eastern flank of the sulfide mound hosts a dense field of small (<1 m), active (white) and inactive (brown) barite chimneys (Fig. 2). The barite chimneys are characterized by several porous branches and are typically covered by white cotton-like bacterial mats. The adjacent black anoxic sediment is densely populated by tube-building polychaetes, i.e., *Nicomache lokii* sp.nov, providing a stable substrate for a range of invertebrates in this vent field (Kongsrud and Rapp 2012). The temperature of clear shimmering fluids locally seen to emanate from this low-temperature field was measured to be approximately 20 °C, while ambient deep water was −0.8 °C (Pedersen et al. 2010). The vent fluid chemistry of these low-temperature fluids indicates a mixing of seawater with at least 10 % high-temperature fluid, but an additional contribution of microbial sulfate reduction in the sub-seafloor of the hydrothermal mound was suggested based on multiple sulfur isotope analyses (Eickmann et al. 2014). For this study we subsampled a white porous barite chimney that

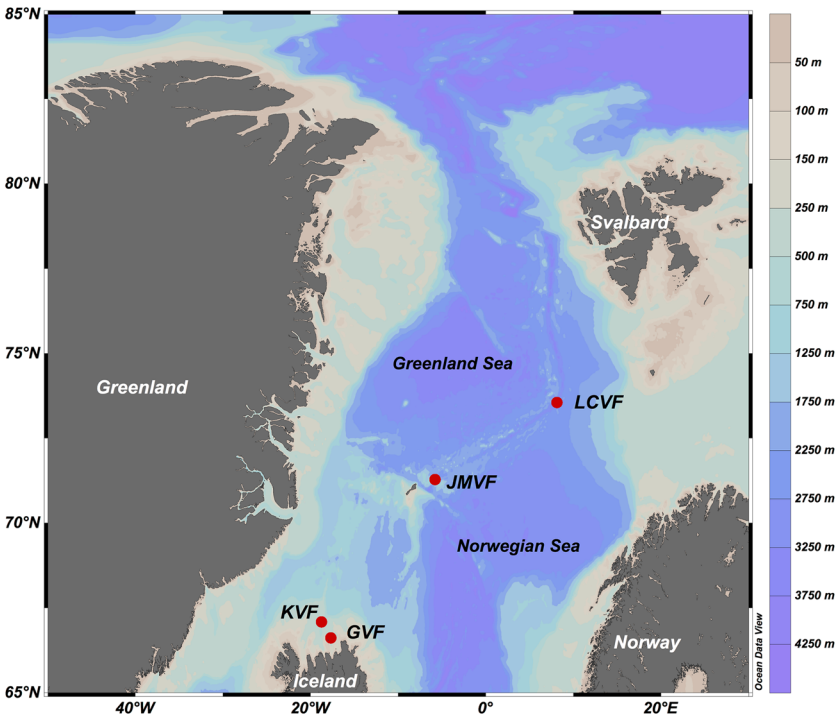

Fig. 1 Location of the Loki's Castle hydrothermal vent field (LCVF) in relation to other known vent fields along the Arctic Mid-Ocean Ridge system. JMVF: Jan Mayen vent field, GVF: Grimsey vent field, KVF: Kolbeinsey vent field. Map was created using the ODV software (Schlitzer 2013)

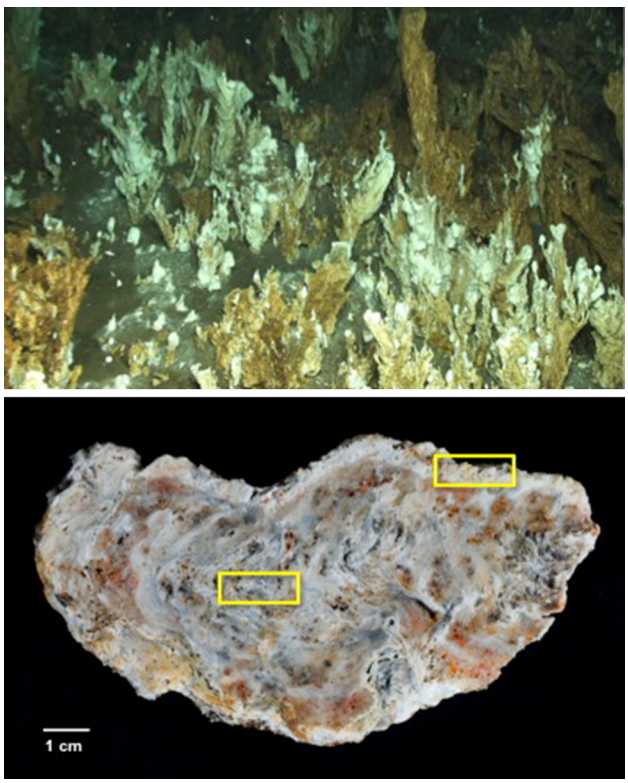

Fig. 2 **a** Small (<1 m) active (*white*) and inactive (*brown*) barite chimneys associated with white microbial mats and siboglinid tubeworms at the low-temperature diffuse venting area at Loki's Castle; **b** cross section of the extinct chimney. The internal structure is dominated by amorphous silica and exhibits several small channels. The outer rim is dominated by white porous barite. *Squares* indicate where subsamples were taken

was actively venting (GS09-ROV7-1: exterior branch; GS09-ROV7-2: interior part with black flow channel material), soft black surface sediment (GS10-ROV4) as well as a massive barite-bearing silica chimney (GS10-ROV8) (Table 1). The silica–barite chimney was about 40 cm in length and 10 cm in diameter and already inactive when sampled (Fig. 2b). Two discrete zones were taken for further analysis, a white porous outer layer (GS10-ROV8-1) and the dense interior zone (GS10-ROV8-2). No central fluid conduits were visible; however, several small channels were identified within the structure. Weathering/oxidation features were visible at the outer rim of the chimney. All samples were collected with a Bathysaurus XL remote operating vehicle (ROV) using an aluminum scuffle box and stored at −20 °C.

Bulk analyses

Freeze-dried, crushed, and powdered chimney samples were subjected to X-ray diffraction (Bruker, AXS D8 Advance apparatus) to determine the mineral composition. Total organic carbon abundance (TOC) and carbon and sulfur isotope ratios ($\delta^{13}C_{TOC}$ and $\delta^{34}S$, respectively) of bulk chimney material (Table 1) were measured after decarbonation on a ThermoFisher Flash-EA 1112 elemental analyzer coupled via a Conflo IV interface to a ThermoFisher Delta V isotope ratio mass spectrometer. The system was calibrated with the reference materials NBS22 ($\delta^{13}C = -30.03$ ‰) and IAEA CH-6 ($\delta^{13}C = -10.46$ ‰) for carbon, and NBS 127 ($\delta^{34}S = +21.1$ ‰),

Table 1 Dive information and bulk data of chimneys and sediment from Loki's Castle low-temperature vent field at the Arctic Mid-Ocean Ridge

Year-dive number-subsample	TOC (%)	$\delta^{13}C$ (‰)	$\delta^{34}S$ (‰)	Vent type—sample material
2009-GSROV7-1	0.20	−17.9	24.7	A—white porous barite (exterior chimney branch)
2009-GSROV7-2	0.37	−28.7	29.8	A—white barite, flow channel material (chimney interior)
2010-GSROV8-1	0.75	−12.5	18.5	I—white porous barite and Fe-oxides (chimney exterior)
2010-GSROV8-2	0.07	−24.8	n.a.	I—amorphous silica (chimney interior)
2010-GSROV4	1.36	−26.1	−4.9	Black sediment below chimneys

n.a. not analyzed, *A* active, *I* inactive

IAEA-SO-5 ($\delta^{34}S = +0.49$ ‰) and IAEA-SO-6 ($\delta^{34}S = -34.05$ ‰) for sulfates. Measurements were performed at the Geological Institute of ETH Zurich, Switzerland. All analytical results are reported in the usual δ notation, in per mil relative to the Vienna Pee Dee belemnite (VPDB) standard for carbon and the Vienna Canon Diablo troilite (VCDT) standard for sulfur.

Multiple sulfur isotopes ($\delta^{34}S$, $\Delta^{33}S$) of barite

A transect of ten subsamples across the extinct silica–barite chimney was analyzed for $\delta^{34}S$ and $\Delta^{33}S$. For all samples barite was extracted and converted to silver sulfide (Ag_2S) using Thode solution ($HI + HCl + H_3PO_4$) (Thode et al. 1961). Approximately, 2 mg Ag_2S was subsequently converted to sulfur hexafluoride (SF_6) via fluorination in nickel tubes (Ono et al. 2006). The SF_6 was cryogenically and chromatographically purified before introducing into a ThermoScientific MAT 253 mass spectrometer via a dual inlet system and the ^{32}S, ^{33}S and ^{34}S isotopes were measured simultaneously. The results are reported in the δ-notation:

$$\delta^{3X}S = \left[\left({}^{3X}S/{}^{32}S_{Sample}\right) - \left({}^{3X}S/{}^{32}S_{V-CDT}\right)\right] / \left({}^{3X}S/{}^{32}S_{V-CDT}\right) \times 1000(‰)$$

where ^{3X}S is ^{32}S, ^{33}S or ^{34}S. The Vienna Canyon Diablo Troilite is defined by IAEA S-1 ($\delta^{33}S = -0.055$ and $\delta^{34}S = -0.300$ ‰), which was used as standard (Ono et al. 2007). $\Delta^{33}S$ values were calculated from $\delta^{33}S$ and $\delta^{34}S$ values:

$$\Delta^{33}S = \delta^{33}S - 1000 \times \left(\left(1 + \delta^{34}S/1000\right)^{0.515} - 1\right)$$

Multiple sulfur isotope measurements were performed at the Institut für Geologie und Paläontologie in Münster, Germany. All samples were reproduced within 0.3 ‰ for $\delta^{34}S$ and 0.02 ‰ for $\Delta^{33}S$ (1σ).

Lipid extraction, derivatization, and fractionation

Freeze-dried and homogenized sample material (GS10-ROV8-1: 3.3 g; GS10-ROV8-2: 47.7 g; GS09-ROV7-1: 147.8 g; GS09-ROV7-2: 25.2 g; GS10-ROV4: 18.6 g) was ultrasonically extracted 3× using methanol (MeOH), dichloromethane (DCM)/MeOH (1:1 by volume), and DCM. The bulk of the solvent was rotarily evaporated and the total lipid extract (TLE) further dried over a Na_2SO_4 column. An aliquot was methylated with MeOH/HCl (10 % w/v) at 70 °C for 2 h to convert fatty acids into their corresponding methyl esters (FAMEs) and silylated with bis(trimethylsilyl) trifluoro-acetamide (BSTFA) in pyridine at 60 °C for 20 min to convert alcohols in trimethylsilyl (TMS) ether derivatives. The position of the double bonds in the fatty acids was determined by analysis as their dimethyl disulfide (DMDS) adducts according to Elvert et al. (2003). Briefly, an aliquot of the sample dissolved in 50 µl *n*-hexane was treated with 100 µl DMDS and 20 µl of iodine solution (6 % w/v in diethyl ether). The reaction was carried out in 2 ml screw-cap glass vials at 50 °C for 48 h. The mixture was cooled and diluted with 500 µl *n*-hexane. The excess of iodine was reduced by addition of 500 µl sodium thiosulfate (5 % w/v in MilliQ water). The organic phase was removed and the aqueous phase extracted twice with 500 µl of *n*-hexane. Combined organic phases were evaporated under a stream of nitrogen and diluted with 100 µl *n*-hexane prior to GC–MS analysis. An aliquot of the TLE was chromatographically separated over activated using *n*-hexane/DCM (9:1 v/v) and DCM/MeOH (1:1 v/v, 3 column volumes) to elute the apolar and polar fractions, respectively. The polar fractions containing GDGTs were redissolved in HPLC-grade *n*-hexane/isopropanol (99:1 v/v) and filtered through a 0.45 µm PTFE filter prior to HPLC/APCI/MS analysis.

Analysis and identification of biomarkers

High-performance liquid chromatography–mass spectrometry (HPLC–MS)

GDGT analysis was performed using high-performance liquid chromatography/atmospheric pressure chemical ionization–mass spectrometry (HPLC/APCI–MS) with a Thermo Surveyor LC system coupled to an LCQ Fleet ion

trap mass spectrometer equipped with a PAL LC autosampler and Xcalibur software, as described by Hopmans et al. (2000). Normal phase separation was achieved with an Alltech Prevail Cyano column (150 mm × 2.1 mm; 3 μm) maintained at 30 °C. The flow rate of the *n*-hexane:isopropanol (IPA) (99:1) mobile phase was 0.3 ml min^{-1}, isocratically for the first 5 min, thereafter with a linear gradient to 2 % IPA in 30 min, and a column cleaning step with 10 % IPA in *n*-hexane. The injection volume was 20–50 μl. Scanning was performed over the *m/z* ranges 650–656, 740–746, 1016–1054 and 1280–1318. The relative abundances of GDGTs were calculated using peak areas of the $[M+H]^+$ ions vs. those of the C_{20}-diol internal standard (*m/z* 743). GDGTs were identified and distinguished via their MS^2 spectra. MS^2 experiments were performed with conditions according to Knappy et al. (2009). Briefly, eluting species were monitored using the positive ionization mode of the APCI source. Conditions for APCI–MS were as follows: vaporizer temperature 300 °C, sheath gas (N_2) flow rate 40 (arb. units), auxiliary gas (N_2) flow rate 5 (arb. units), capillary temperature 200 °C, capillary voltage 23 V, corona discharge current 5 μA. Positive ion MS spectra were obtained by scanning a narrow mass range from *m/z* 1220 to 1350. MS^2 spectra were recorded using the data-dependent ion scan feature, in which the base peak of an MS scan is selected for collision-induced dissociation (CID) in MS^2 (collision energy was set at 30 %).

Gas chromatography–mass spectrometry (GC–MS) and GC-isotope ratio mass spectrometry (irm) MS

Compound identification was done by combined gas chromatography–mass spectrometry (GC–MS). GC–MS was conducted using a Hewlett Packard 6890 gas chromatograph equipped with an on-column injector. A fused silica capillary column (HP-5, 30 m length, 0.25 mm inner diameter, 0.25 μm film thickness) with helium as a carrier gas was used. The gas chromatograph was interfaced to an HP 5973 mass selective detector (MSD) with a mass range of *m/z* 50–800. The samples were injected at 60 °C. The GC oven temperature was subsequently raised to 120 °C at a rate of 10 °C min^{-1} and then to 320 °C at 4 °C min^{-1}. The temperature was then held constant for 20 min. The structural characterization of lipids was evaluated by comparing their mass spectral fragmentation pattern with published spectra. Carbon isotopes were measured using a Thermo Scientific system with a Trace GC Ultra, a GC IsoLink interface, a Conflo IV, and a Delta V Plus isotope ratio monitoring mass spectrometer. The GC equipped with a DB-1 fused silica column was programmed as described above. Each sample was measured at least twice. $\delta^{13}C$ values are expressed in ‰ relative to VPDB. Correction was done for carbon added during derivatization. The reproducibility based on multiple analysis of samples was better than ±1 ‰.

Results and discussion

Reconstruction of chimney formation and cooling history

The inactive chimney recovered from the low-temperature area at Loki's Castle (Table 1; Fig. 2) consisted almost entirely of amorphous silica and barite, while Fe-oxides were minor constituents of the outer rim, and sulfides were lacking. The amorphous silica was largely intergrown with barite. The precipitation of silica is controlled by the pH, temperature, and pressure of the fluids. The formation of amorphous silica in hydrothermal systems is most likely the result of a combination of mixing between seawater and a hydrothermal fluid and subsequent conductive cooling of this mixture (Hannington and Scott 1988; Herzig et al. 1988; Shanks et al. 2007). To precipitate amorphous silica, a hydrothermal fluid with a temperature of ~350 °C and a high Si content is required (Herzig et al. 1988). The Si concentrations of the Loki's Castle high-temperature hydrothermal fluids (305–317 °C), which emanate ~50 m in the westerly direction from the low-temperature venting area, ranges from 14.6 to 16.3 mmol kg^{-1} (Baumberger 2011; Pedersen et al. 2010). When these ascending silica-saturated fluids discharge into the cold seawater, amorphous silica precipitates to form small chimneys. The chimney formation is most likely facilitated along cracks or fractures in the seafloor. Once the amorphous silica solidifies at the seafloor, a barrier between the hydrothermal fluid and surrounding seawater is established that precludes further mixing between both fluids. Hence, this barrier enhances further silica precipitation that results in fast chimney growth (Shanks et al. 2007). The existence of small flow channels in the silica matrix suggests that the silica–barite chimney is an actively venting chimney. Furthermore, the lack of sulfide minerals indicated that the fluid from which the silica precipitated was below 350 °C, which is insufficient for leaching metals from basalts or sulfide precipitation below the seafloor (Janecky and Seyfried 1984).

Most of the signatures from the interior and exterior of the inactive silica chimney fell in a tight range for both $\delta^{34}S_{Barite}$ (+21.1 to +22.5 ‰) and $\Delta^{33}S_{Barite}$ (+0.019 to +0.034 ‰) (Table 2; Fig. 3). This multiple sulfur isotopic composition indicates a major if not exclusive contribution of seawater sulfate ($\delta^{34}S = +21.3$ ‰, $\Delta^{33}S = +0.050$ ‰). Seawater penetrated into the silica matrix likely along cracks, former flow channels and along pores, followed by barite precipitation. The homogeneity in the sulfur isotopic composition close to the seawater value suggests no further modification of the original seawater

Table 2 Multiple sulfur isotope compositions of barite from the inactive chimney (GS10-ROV8, subsamples 1–10), ambient seawater, and microbial mats from active barite chimneys normalized to the VCDT scale

Sample	Material	$\delta^{34}S$ (‰)	$\Delta^{33}S$ (‰)
GS10-ROV8-1[a]	Barite	n.a.	n.a.
GS10-ROV8-2[b]	Barite	9.7	−0.014
GS10-ROV8-3[b]	Barite	n.a.	n.a.
GS10-ROV8-4[b]	Barite	22.3	0.024
GS10-ROV8-5[b]	Barite	21.6	0.034
GS10-ROV8-6[b]	Barite	21.1	0.031
GS10-ROV8-7[b]	Barite	22.5	0.019
GS10-ROV8-8[b]	Barite	21.0	0.025
GS10-ROV8-9[b]	Barite	21.3	0.020
GS10-ROV8-10[a]	Barite	22.5	0.029
GS09-CTD7-2[c]	Seawater	21.3	0.020
GS09-CTD84[c]	Seawater	21.2	0.040
GS10-ROV5BS-1	Barite/mat	21.1	0.020
GS10-ROV5BS-2	Barite/mat	20.4	0.013

n.a. not analyzed, *BS* biosyringe

[a] Chimney exterior

[b] Chimney interior

[c] Data from Eickmann et al. (2014)

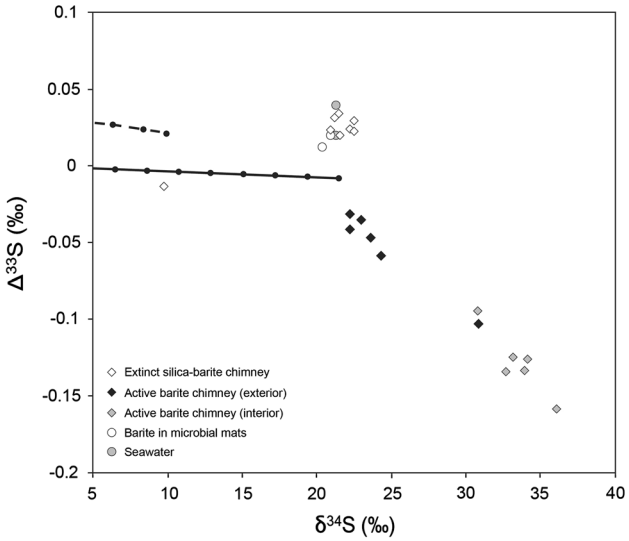

Fig. 3 $\delta^{34}S$ versus $\Delta^{33}S$ values for sulfate from the inactive barite-bearing silica chimney (*open diamonds*; this study), microbial mats associated with actively venting barite chimneys (*open circles*; this study), an active barite chimney GS09-ROV7 (*filled diamonds*), and ambient seawater (*filled circles*) from the Loki's Castle vent field (data from Eickmann et al. 2014). The *solid line* represents mixing of basaltic sulfide and seawater sulfate, whereas the *dashed line* shows isotope composition of H_2S that is in isotope equilibrium with seawater sulfate as a function of temperature (see Ono et al. 2007)

signature (Paytan et al. 2002). In contrast, the porous outer barite layer of the inactive silica–barite chimney reveals a slightly lower sulfur isotope ratio ($\delta^{34}S = +18.5$ ‰; Table 1) than ambient seawater sulfate, suggesting the admixture of sulfate from a different source. This value resembles values recorded for barite from modern hydrothermal settings (Noguchi et al. 2011; Paytan et al. 2002; Torres et al. 2003) as well as for barite from a similar silica–barite chimney from the Sumisu Rift (Urabe and Kusakabe 1990). Moreover, the multiple sulfur isotopic composition for most of the barite in the chimney is similar to that from microbial mats associated with actively venting barite chimneys from the same low-temperature vent area at Loki's Castle (Fig. 3). Hence, barite with a marine sulfur isotopic composition seems to be the dominant type in the Loki's Castle vent field. A $\delta^{34}S$ value of +9.7 ‰ and a $\Delta^{33}S$ value of −0.014 ‰ recorded for a barite subsample from the chimney interior are distinctly different in its multiple sulfur isotopic composition and could be indicative of mixing between a hydrothermal fluid and seawater.

In contrast to the silica–barite chimney, the sulfur isotope signatures from an actively venting barite chimney collected in the same low-temperature area cannot be explained by simple mixing of seawater with hydrothermal fluid, as has been reported by Eickmann et al. (2014). The $\delta^{34}S$ values of bulk material from the barite chimney were 24.7 ‰ in the exterior branch (GS07-ROV7-1) and 29.8 ‰ in the interior part (GS09-ROV7-2), thus substantially heavier compared to the extinct silica–barite chimney (Table 1). This contrast became even more evident by multiple sulfur isotope analysis of subsamples from the exterior and interior of the same chimney. $\delta^{34}S$ values up to +36.1 ‰ and $\Delta^{33}S$ values as low as −0.159 ‰ were recorded from the interior part of the barite chimney (Fig. 3) and are clearly different from ambient seawater, thus indicating that barite precipitated from a fluid that had been modified by microbial sulfate reduction in the underlying sediment (Eickmann et al. 2014). Further support for sulfate reduction was provided directly from the adjacent black sediment, which had a $\delta^{34}S_{bulk}$ value of −4.9 ‰ (Table 1). There, abundant framboidal pyrite with a distinct sulfur isotopic composition ($\delta^{34}S = -16.4$ ‰, $\Delta^{33}S = +0.115$ ‰) also pointed to a biogenic origin (Eickmann et al. 2014). In the following sections, we will explore major microbial signatures in the barite and silica structures as well as in the sediment by means of biomarker lipid and compound-specific carbon isotope analysis.

Heterogeneity of microbial signatures in the silica and barite chimney structures

Biomarker lipid analysis of inactive and active chimney material and black sediment showed substantial differences in biomarker content per gram dry weight, ranging from 0.9 to 7.5 μg g^{-1}. The microbial communities, as reflected

Table 3 Abundances (ng g^{-1} dry material) of biomarkers extracted from silica and barite chimneys as well as hydrothermal sediment from Loki's Castle low-temperature vent area

Core lipid class	Compound (*m/z*)	Si–Ba chimney, inactive		Ba chimney, active		Black sediment
		ROV8-1 Exterior	ROV8-2 Interior	ROV7-1 Exterior	ROV7-2 Interior	ROV4
GTGT	1304	2.68	10.07	0.14	nd	0.20
Iso-GDGT	GDGT-0 (*1302*)	284.86	544.84	12.68	323.31	27.43
	GDGT-1 (*1300*)	20.55	148.03	2.25	42.68	1.35
	GDGT-2 (*1298*)	14.28	217.73	2.85	45.64	0.55
	GDGT-3 (*1296*)	17.99	312.42	1.16	17.07	0.36
	GDGT-4 (*1294*)	46.98	380.63	0.38	nd	nd
	Crenarchaeol (*1292*)	104.90	32.91	0.87	129.46	20.72
	Cren isomer (*1292′*)	1.04	nd	0.01	0.96	0.08
GMGT	GMGT-0 (*1300*)	195.26	1123.81	nd	nd	0.65
	GMGT-1 (*1298*)	29.63	341.93	nd	nd	nd
	GMGT-2 (*1296*)	23.35	318.44	nd	nd	nd
	GMGT-3 (*1294*)	11.02	140.85	nd	nd	nd
	GMGT-4 (*1292*)	73.32	535.71	nd	nd	nd
Br-GDGT	(*1022*)	3.50	10.20	0.16	nd	nd
	(*1020*)	nd	nd	nd	11.93	0.41
	(*1018*)	nd	nd	nd	10.70	0.35
	(*1036*)	5.18	10.92	0.23	2.27	nd
	(*1034*)	nd	nd	nd	12.40	0.94
	(*1032*)	nd	nd	nd	nd	0.20
	(*1050*)	2.47	5.66	0.16	nd	nd
Isoprenoid hydrocarbons/ diethers	Crocetane	nd	147	nd	nd	nd
	PMI	nd	29	nd	nd	nd
	Archaeol	nd	478	10.4	nd	nd
	sn-2-OH-Ar	nd	102	nd	nd	nd
Fatty acids	*i*-$C_{15:0}$	165.4	nd	7.7	15.90	152.7
	ai-$C_{15:0}$	199.8	nd	7.9	29.94	150.1
	$C_{15:0}$	nd	nd	3.5	17.12	nd
	i-$C_{16:0}$	126	nd	3.3	18.76	nd
	$C_{16:1\omega7c}$	2084.7	nd	366.6	869.91	892.4
	$C_{16:1\omega5c/t}$	303.4	nd	45.9	117.31	286.0
	$C_{16:0}$	1587.7	nd	105.3	99.62	344.5
	10-Me-$C_{16:0}$	354.1	nd	3.1	27.07	89.7
	$C_{17:1w6}$	nd	nd	9.5	nd	nd
	i-$C_{17:0}$	171.8	nd	nd	33.70	56.7
	ai-$C_{17:0}$	261.9	nd	nd	nd	nd
	$C_{17:0}$	nd	nd	6.2	nd	nd
	$C_{18:2}$	nd	nd	14.7	nd	nd
	$C_{18:1\omega9c}$	260.4	nd	32.0	10.05	176.4
	$C_{18:1\omega7c/t}$	676.8	nd	139.1	252.84	385.3
	$C_{18:0}$	444.7	nd	80.0	65.3	148.7

nd not detected, *PMI* pentamethylicosane, *GTGT* glycerol trialkyl glycerol tetraether, *GDGT* glycerol dialkyl glycerol tetraether, *GMGT* glycerol monoalkyl glycerol tetraether ('H-shaped' GDGT)

by lipid biomarkers, also differed substantially (Table 3). In the extinct silica–barite chimney, where the mineral composition indicated a zonation into distinct habitats for microorganisms, total lipid concentration was about 1.5 times higher in the exterior zone (7.5 μg^{-1}) than in the chimney interior (4.9 $\mu g\ g^{-1}$). This represents a high microbial density in the extinct chimney, which is higher than those of both the actively venting barite chimney and the sediment from the same vent field (Table 3), in agreement with findings by Kato et al. (2010).

Reconstruction of potential source organisms in the inactive silica–barite chimney indicated the dominance of bacteria in the exterior zone, where fatty acids contributed 89 % to the total lipid pool. Archaea were the predominant organisms in the chimney interior as revealed by a dominance of archaea-specific tetraether lipids (Table 3). Microbial activity is likely to be higher in the exterior parts that are exposed to seawater than in the chimney interior reflecting the availability of organic carbon, sulfide sulfur, and oxygen as favorable carbon and energy sources (McCollom and Shock 1997; Kato et al. 2010). This is in contrast to the active barite chimney, where highest biomarker concentration was found toward the interior (2.2 $\mu g\ g^{-1}$) and close to the fluid flow channels, while it was 0.85 $\mu g\ g^{-1}$ in the highly porous outer branch of the barite. Bacteria were the dominant organisms in the active barite contributing 97.5 % of the total lipids in the exterior and 62.5 % in the interior. Similarly, high abundance and dominance of bacteria were also observed in the black sediment, where the total concentration of detected lipids was 2.8 $\mu g\ g^{-1}$, and of these 98.1 % were bacterial. The carbon isotope composition of the total organic carbon ($\delta^{13}C_{TOC}$) was −12.5 and −17.9 ‰ in the exterior chimney barite, while it was distinctly more negative in the interior parts of both chimneys (−24.8 and −28.7 ‰, respectively) as well as in the black sediment (−26.1 ‰) (Table 1). These differences could point to carbon sources with different $\delta^{13}C$ contents or a change in the dominance of the carbon fixation pathway within the microbial community. The actual biomarker inventory of the chimneys and sediment includes compounds beyond fatty acids and ether lipids, such as high abundances of C_{27}−C_{29} sterols detected mainly in the black sediment and the interior of the active barite chimney. These eukaryotic sterols are most likely derived from the rich vent fauna, i.e., tube-building polychaetes that are thought to be grazers and were independently determined to have a $\delta^{13}C_{Biomass}$ of −22.5 ‰ (Kongsrud and Rapp 2012). While these compounds undoubtedly contribute to the bulk $\delta^{13}C_{TOC}$ signatures, we focus here on the major microbial core lipids detected in the low-temperature vent habitat at Loki's Castle.

When CO_2 was the primary carbon source for microbial biosynthesis, the isotopic offset with bulk biomass varied between 5.8 and 22 ‰ for all samples. At the fluid pH of 5.5, over 80 % of the dissolved inorganic carbon (DIC) will be in CO_2 form. The relatively small offset between CO_2 and biomass in the exterior of the two chimney samples may point to the dominance of a carbon fixation pathway that does not discriminate strongly against ^{13}C, such as the reductive tricarboxylic acid cycle or the 3-hydroxypropionate cycle (House et al. 2003).

Distribution and origin of archaeal and bacterial tetraether lipids

HPLC–MS analysis of chimney material revealed the presence of isoprenoid mono-, di-, and trialkyl tetraether lipids (Fig. 4), as well as archaeol and hydroxyarchaeol, indicating diverse consortia of archaea in the samples from the low-temperature venting area (Table 3). GMGTs ('H-shaped' GDGTs) with up to four cyclopentane rings were the dominant compounds detected in the interior of the inactive silica–barite chimney, contributing nearly 60 % to the total tetraether core lipid pool (Fig 5). The relative distribution of GMGTs was similar in the chimney exterior to this sample, but had lower total abundances (Table 3). An isoprenoid cross-linking in archaeal tetraether lipids was suggested to provide more rigidity to the cell membrane at high temperatures (Schouten et al. 2008a; Uda et al. 2004). Indeed, these rather unusual lipids were so far reported for cultivated isolates of extremophilic archaea that can grow at temperatures well above 100 °C (Knappy et al. 2009, 2011; Morii et al. 1998; Schouten et al. 2008a; Sugai et al. 2004) as well as in a black smoker chimney wall (Jaeschke et al. 2012). Among the archaea detected in black smokers of the main vent field of Loki's Castle, hyperthermophilic sulfur-reducing *Thermococcaceae* were dominant (28.4 % of the total 16S rRNA pool). Other less abundant archaea belonged to the classes *Methanococci, Archaeoglobi, Thermoprotei*, and *Thermoplasmata* (Jaeschke et al. 2012). Reduction of elemental sulfur is one of the most common reactions by which many different isolates of thermophilic archaea can be grown in the laboratory (Amend and Shock 2001; Blöchl et al. 1995; Schönheit and Schäfer 1995). The oxidation and reduction of elemental sulfur and reduced inorganic sulfur species are some of the most important energy-yielding reactions for microorganisms living in sulfide-rich deep-sea hydrothermal vent ecosystems, including both heterotrophic, mixotrophic, and chemolithoautotrophic carbon dioxide-fixing species (Kletzin et al. 2004), and likely very ancient metabolisms (Canfield and Raiswell 1999). GMGTs have also been reported as the main membrane lipids of *Methanothermus* (Koga and Morii 2005). Methanogenic archaea and especially the (hyper-)thermophilic members of the genera *Methanopyrus, Methanobacterium, Methanothermus*, and *Methanococcus*

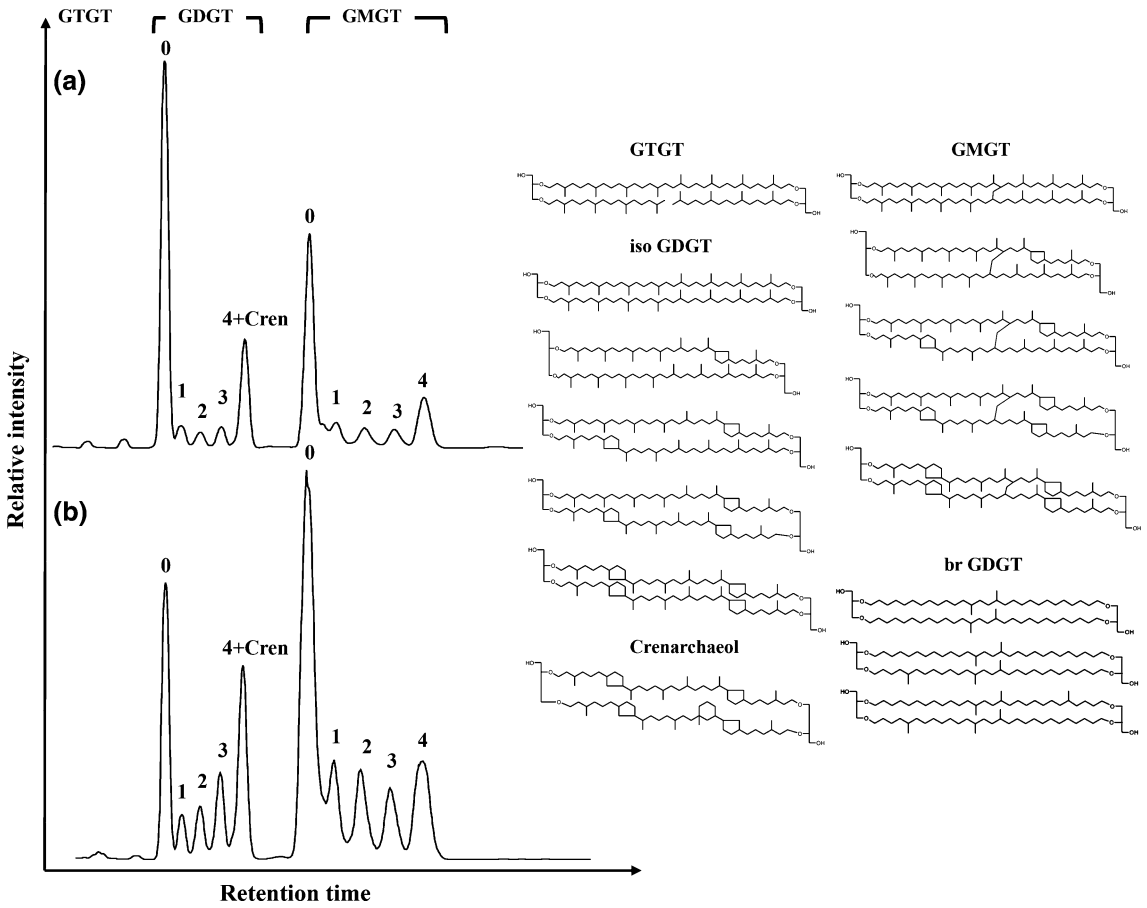

Fig. 4 HPLC/APCI/MS base peak chromatogram showing the distribution of tetraether lipids detected in the **a** exterior and **b** interior of an inactive silica–barite chimney. Different lipid classes were distinguished via their MS2 spectra. Low abundances of branched GDGTs are masked by GMGTs. Numbers indicate the amount of cyclopentane rings in the structure. *Cren* crenarchaeol. Molecular structures of tetraether core lipids detected in the extinct silica–barite chimney (see text). *GTGT* glycerol trialkyl glycerol tetraether; *GDGT* glycerol dialkyl glycerol tetraether; *GMGT* glycerol monoalkyl glycerol tetraether ('H-shaped' GDGT). The position of the covalent bond in the GMGTs is tentative (Morii et al. 1998)

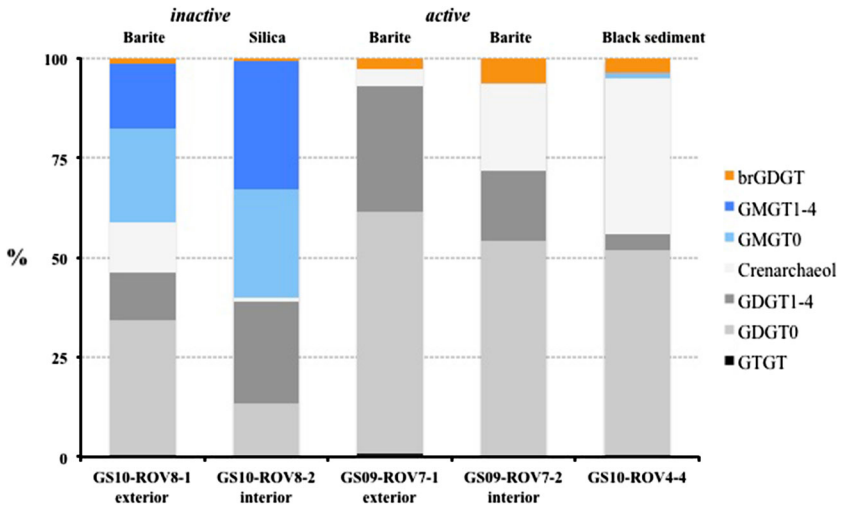

Fig. 5 Relative abundances of archaeal and bacterial tetraether lipids present in chimney structures and sediment at Loki's Castle low-temperature venting area

produce significant amounts of H_2S in the presence of S^0, while the rate of methanogenesis is reduced (Stetter and Gaag 1983). Members of thermophilic *Thermoprotei* and *Methanobacteria* have also been suggested to be the likely source for GMGT's (predominantly GMGT-0) detected at Lost City (Lincoln et al. 2013). The presence of methanogenic archaea would also partly explain the high abundances of GDGT-0 and archaeol (including hydroxyarchaeol) detected in the interior zone of the chimney (Table 3) (Koga and Morii 2005; Koga and Nakano 2008). GMGT-0 present in marine and lacustrine sediments also suggests a non-hydrothermal ($T < 35$ °C) source for this compound (Schouten et al. 2008b). Indeed, GMGT-0 was detected in low abundance (1.2 % of total tetraether lipids) in the black sediment of the low-temperature vent field, while GMGT's were generally absent in the active barite chimney (Table 3; Fig. 5). Thus, GMGT-0 may be produced by some benthic archaea as suggested by Schouten et al. (2008b), while GMGTs with up to four rings as detected in the extinct silica–barite chimney are most likely derived from a different group of hyperthermophilic archaea.

Despite enormous differences in total abundances, isoprenoid GDGTs with 0–4 rings were present in high relative abundances accounting for 39 % in the silica chimney and up to 92 % in the porous barite chimney branch (Table 3; Fig. 4). All major archaeal groups have the potential to synthesize GDGTs detected in the samples; thus it is difficult to link them to specific source organisms. However, GDGT-0 is the main membrane lipid of methanogens, while methanotrophic archaea of the ANME-1 phylogenetic cluster may be an important source of GDGTs 1–4 (Blumenberg et al. 2004; Pancost et al. 2000; Schouten et al. 2003). Indeed, 16S rRNA gene sequence analysis revealed that anaerobic methanotrophs (ANME) of the ANME-1 clade and the GOM-arc1 group were dominating in the white chimney barite, while the microbial community structure was more diverse in the fluid flow channels within the barite (Steen et al. 2011). However, the highly porous barite chimney structure suggests that the presence of ANME-1 archaea may be restricted to anoxic microniches.

While GDGTs 0–3 were abundant in all samples, GDGT-4 was only detected in the extinct silica–barite chimney as well as in the outer branch of the active barite chimney (Table 3). In general, the number of cyclopentane rings incorporated in tetraether lipids increases with increasing growth temperature (i.e., Boyd et al. 2011; Schouten et al. 2002; Uda et al. 2001). Indeed, abundances of ring-containing GDGTs and GMGTs are substantially higher in the warm interior zone compared to the outer zone (Fig. 5). Moreover, the dominance of GDGTs 1–4 over crenarchaeol in the chimney interior may indicate a strong input of (hyper-)thermophilic *Crenarchaeota*, which has been reported for hot springs (Burgess et al. 2012; Pearson et al. 2004; Zhang et al. 2006), while crenarchaeol (including its regio-isomer) and GDGT-0 were detected in higher relative abundance in the chimney exterior as more commonly observed for cultivated *Thaumarchaeota* (see section below). However, despite the possibly high temperatures in the chimney interior, we did not detect GDGTs/GMGTs with more than four rings. GDGTs with up to eight rings were reported for Yellowstone hot springs with temperatures of up to 83 °C (Schouten et al. 2007). Thus, the specific lipid distribution in thermophilic archaea may reflect the adaptation to the extreme local conditions controlled by pH, pressure, or heavy metal content. Lai et al. (2008) showed that the tetraether to diether ratio increased with increasing growth temperature in *Archaeoglobus fulgidus*, while the number of rings did not exceed two pentacycles. Indeed, besides higher abundances of ring-containing GDGTs in the warmer interior zone of the chimney, archaeol (including *sn*-2-hydroxyarchaeol) was detected accounting for 12 % of the total lipids, while it was lacking in the chimney exterior (Table 3). Archaeol, an isoprenoid diether, was also detected in the exterior branch of the active barite in similar concentration as caldarchaeol (Table 3). Archaeol is rather unspecific as it is produced by various archaeal groups including methanogens (Koga and Morii 2005; Koga and Nakana 2008), while hydroxyarchaeol was reported as a major lipid of ANME-2 archaea (Blumenberg et al. 2004).

Crenarchaeol was detected in all samples with highest relative abundances in the black sediment (39 %) and chimney barite with flow channel material (22 %), while it contributed only 4 % to the tetraether pool in the outer branch of the active barite chimney (Table 3). In the extinct silica–barite chimney, crenarchaeol was abundant in the exterior zone (12.7 %), while it was a minor compound in the interior part (0.8 %). The crenarchaeol regio-isomer was also detected in all samples except for the interior of the extinct silica–barite chimney. Marine group I *Thaumarchaeota* (MGI) may be the likely source for crenarchaeol detected in our samples (Steen et al. 2011). Crenarchaeol has been postulated as a specific biomarker for ammonia-oxidizing archaea (AOA) including marine group I.1a and terrestrial group I.1b (De la Torre et al. 2008; Pitcher et al. 2010). Initially thought to be produced solely by mesophiles, crenarchaeol synthesis was later also confirmed for thermophiles (De la Torre et al. 2008; Pearson et al. 2004; Zhang et al. 2006). High ammonia (and methane) concentrations detected in the vent fluids of Loki's Castle, which strongly indicate a sedimentary component below the volcanic ridge (Pedersen et al. 2010), may support the presence of (thermophilic) AOA in this system. Low abundances of crenarchaeol detected in the

chimney interior that most likely experienced high temperatures may be derived from uncultivated representatives of hyperthermophilic *Crenarchaeota* rather than MGI. This could also explain the lack of the crenarchaeol regio-isomer.

Branched GDGTs (brGDGT) with 0–2 rings were also detected in all samples with 0.6–6.3 % of total tetraethers, however, with different distribution patterns of the individual isomers (Table 3). Both the active and inactive chimney barite contained brGDGTs without additional rings, while they were detected with one and two rings in the black sediment. The active barite chimney with black channel material contained brGDGTs with 0–2 rings. This may indicate an adaptation of the organisms to the very local environmental conditions within the black sediment, the flow channels and chimneys. Initially, brGDGTs were predominantly found in soils and also abundant in coastal marine settings, and their synthesis was attributed to anaerobic soil bacteria (Weijers et al. 2007), possibly *Acidobacteria* (Sinninghe Damsté et al. 2011). So far, there is no reported evidence for the in situ production of brGDGTs in the open oceans, deep-sea sediments, or even hydrothermal vent sites; however, biosynthesis in the water column by yet unknown organisms has already been proposed (Schouten et al. 2013 and references therein). Indeed, brGDGTs were recently detected in hydrothermal sediments and chimneys from the Eastern Lau Spreading Center and the Lost City Hydrothermal Field, the latter of which is distant from any potential inputs of terrestrial organic matter (Hu et al. 2012; Lincoln et al. 2013). Possible source organisms in the chimneys and sediment at Loki's Castle may be members of uncultivated thermophilic *Acidobacteria* that are often reported as part of hydrothermal vent microbial communities (Lopez-Garcia et al. 2003). This, however, needs further investigation of the specific membrane composition of cultivated isolates from this deep-sea vent site.

GDGT-based proxies

Both isoprenoid and branched GDGTs form the base for the TEX_{86} temperature proxy (Schouten et al. 2002) and BIT index (Hopmans et al. 2004), which is a measure for terrigenous input to marine sediments. Temperatures calculated using the original equation of Schouten et al. (2002) were 19.3 °C for the black sediment and ranged from 27.2 to 29.1 °C in the chimneys. BIT index values ranged from <0.1 in the sediment to 0.4 in the chimneys. Because the crenarchaeol regio-isomer was lacking in the extinct silica chimney interior, no temperature estimate was available. The calculated sediment temperature is actually close to the value of ~20 °C measured in situ directly on the seafloor (Pedersen et al. 2010). However, actual fluid temperatures in the chimneys may be higher than that. The TEX_{86} temperature proxy is typically used in paleoceanography for the reconstruction of sea (sub-)surface temperatures (SST), but its applicability was recently also tested for deep-sea hydrothermal sediments and chimneys (Hu et al. 2012; Lincoln et al. 2013). Annual mean SSTs at the study area in the Norwegian-Greenland Sea are approximately 6°. Therefore, the TEX_{86} proxy seems to yield reliable 'in situ' temperature estimates for sediment and likely also for chimneys in this low-temperature vent area, which is in contrast to findings from other hydrothermal environments (Hu et al. 2012; Lincoln et al. 2013).

Origin and carbon isotopic composition of isoprenoid diethers and hydrocarbons

GC–MS analysis of the chimney material revealed other isoprenoid compounds of archaeal origin such as archaeol, *sn*-2-hydroxyarchaeol, crocetane, and pentamethylicosane (PMI) as the predominant compounds of the hydrocarbon fraction. They were only detected in the interior part of the extinct silica–barite chimney with concentrations of 478, 102, 147, and 29 ng g^{-1}, respectively (Table 3). Crocetane and *sn*-2-hydroxyarchaeol seem to be related to ANME-2 archaea (Blumenberg et al. 2004), while PMI was reported to be synthesized by methanogens (Risatti et al. 1984). The co-occurrence of PMI and crocetane with archaeol and hydroxyarchaeol was first reported for the Napoli mud volcano and highly depleted ^{13}C values indicated that methanogenic archaea were operating in reverse, thus anaerobically oxidizing methane (AOM) (Pancost et al. 2000). Anaerobic, methanotrophic archaea were indicated as source organisms for these highly ^{13}C-depleted compounds with values as low as −120 ‰ in sediments, and modern and ancient cold seep environments (Bian et al. 2001; Blumenberg et al. 2004; Elvert et al. 1999; Thiel et al. 1999).

In the samples from Loki's Castle, the ^{13}C contents of individual biomarkers had values of −44.8 ‰ for crocetane and −46.3 ‰ for PMI (Table 4) indicating a similar carbon source. Archaeol was also detected in the exterior branch of the active barite chimney and had a $\delta^{13}C$ value of −37.4 ‰. Unfortunately, no $\delta^{13}C_{methane}$ value is available from the low-temperature fluid, but the $\delta^{13}C_{methane}$ was −28 ‰ in the main black smoker fluid (M. Lilley, personal communication). The $\delta^{13}C_{DIC}$ of this low-temperature fluid (at low pH most DIC is present as CO_2) was −6.7 ‰ (T. Baumberger, personal communication), which is different from the main black smoker field where values range between −11.9 and −10.3 ‰ (Baumberger 2011). The depletion of ^{13}C in the lipids relative to DIC as a likely carbon source by 31−40 ‰ points to the presence of

Table 4 Stable carbon isotope ratios ($\delta^{13}C$, ‰ VPDB) of selected compounds present in the silica and barite chimneys and hydrothermal sediment from Loki's Castle low-temperature vent area

Compound	ROV8-1	ROV8-2	ROV7-1	ROV7-2	ROV4
i-$C_{15:0}$	−27.4	nd	−37.0	−34.2	−34.3
ai-$C_{15:0}$	−26.8	nd	−36.7	−34.4	−33.0
$C_{15:0}$	−27.9	nd	nv	nv	−32.2
i-$C_{16:0}$	−27.7	nd	nv	nv	−30.8
$C_{16:1\omega7c}$	−25.5	nd	−34.7	−35.3	−31.4
$C_{16:1\omega5c/t}$	−27.0	nd	−37.0	−39.7	−33.9
$C_{16:0}$	−23.3	nd	−31.9	−35.1	−31.9
10-Me-$C_{16:0}$	nv	nd	−35.7	nv	−31.8
$C_{17:1w6}$	nd	nd	−36.7	nd	nd
i-$C_{17:0}$	nv	nd	nd	nv	−34.1
ai-$C_{17:0}$	nv	nd	nd	nv	nv
$C_{17:0}$	nv	nd	nd	nv	−34.8
$C_{18:2}$	nv	nd	−33.4	nd	nd
$C_{18:1\omega9c}$	−26.3	nd	−36.4	−33.2	−33.2
$C_{18:1\omega7c/t}$	−27.5	nd	−33.9	−35.9	−33.0
$C_{18:0}$	−24.8	nd	−26.7	−27.9	−32.8
Crocetane	nd	−44.8	nd	nv	nd
PMI	nd	−46.3	nd	nd	nd
Archaeol	nd	nv	−37.4	nd	nd
TOC	−12.5	−24.8	−17.9	−28.7	−26.1

Fluid characteristics were T = ~20 °C; pH = 5.4 (Pedersen et al. 2010)

DIC = 4.4 mmol kg^{-1} and $\delta^{13}C$ = −6.7 ‰ (T. Baumberger, personal communication)

Values represent averages of at least two runs that were reproducible within ±1 ‰

nd not determined; *nv* no value due to low concentration or co-elution

methanogenic or methanotrophic archaea. When the methanogenic archaea *Methanosarcina barkeri* was grown in culture with H_2/CO_2, the newly synthesized PMIs and archaeol were isotopically more negative than the starting CO_2 by as much as 47 ‰ (Londry et al. 2008). ^{13}C-depleted GDGTs indicative of anaerobic methanotrophy were reported for hydrothermal sediment of the Guaymas Basin and a carbonate reef from the Black Sea with isotopic differences of ca. 20 and 35 ‰, respectively, assuming methane as the substrate (Blumenberg et al. 2004; Schouten et al. 2003). However, assimilation of primarily DIC instead of methane by thermophilic ANME-1 archaea was recently reported for hydrothermal sediments of the Guaymas Basin (Kellermann et al. 2012).

Distribution and carbon isotopic composition of bacterial fatty acids

Bacterial fatty acids were the most abundant lipids detected in the active barite chimney, the barite exterior of the inactive silica–barite chimney, and the black sediment (Table 3). Except for the interior part of the extinct silica–barite chimney saturated, unsaturated and branched fatty acids in the C_{15} to C_{18} carbon range were detected in all samples. Fatty acids were dominated by $C_{16:1\omega7c}$ (31.4–56 %) and $C_{18:1\omega7c}$ (10.2–16.9 %) that may be derived from sulfur-oxidizing bacteria in this H_2S-rich setting, while generally less abundant $C_{16:1\omega5c}$ (4.6–10.7 %) and $C_{18:1\omega9c}$ (3.9–6.6 %) have also been reported as signature lipids of sulfate-reducing bacteria (SRB) (Elvert et al. 2003, 2005; Guezennec et al. 1998; Zhang et al. 2005). Branched (*iso*- and *anteiso*-) C_{15} (2–9 %) and C_{17} fatty acids (2–7 %) as well as the 10Me-$C_{16:0}$ fatty acid (0.4–5.3 %) may also indicate the presence of sulfate-reducing bacteria (Dowling et al. 1986; Zhang et al. 2005). A respective signal for microbial sulfate reduction based on multiple sulfur isotope data, however, was only discernible for the black sediment and the active barite chimney (Eickmann et al. 2014). Saturated C_{16} (6.4–23.9 %) and C_{18} (5.5–9.7 %) fatty acids are common in many bacteria, and thus rather unspecific. The lipid pattern in the barite exterior of the extinct silica–barite chimney is very similar to that in the active barite chimney of the same low-temperature vent area, thus indicating similar assemblages (Table 3). The white cotton-like mats associated with actively venting barite chimneys on the other hand were dominated by $C_{18:1\omega7c/t}$ (70 %), while $C_{18:0}$ (8 %), $C_{16:1\omega7c}$ (8 %), and $C_{16:0}$ (5 %) fatty acids were less abundant (data not shown). 16S rRNA gene sequence analysis showed that these mats were dominated by *Sulfurimonas*, sulfur-oxidizing chemolithoautotrophs belonging to the ε-Proteobacteria (Steen et al. 2011). Excess H_2S in the low-temperature hydrothermal fluids provided by microbial sulfate reduction in the sub-seafloor of the barite field potentially fuels sulfur oxidation in the chimneys and associated mats (Eickmann et al. 2014). Hydrothermal fluids circulating through basalt are generally enriched in sulfur compounds, and thermodynamic models predict that sulfur oxidation provides the highest amount of energy for microbes at lower ambient temperatures (<35 °C) (McCollom and Shock 1997).

The $\delta^{13}C$ of individual fatty acids ranged from −23.3 to −27.9 ‰ in the inactive chimney barite, and from −26.7 to −39.7 ‰ in the active chimney barite and sediment (Table 4). All fatty acids were depleted in ^{13}C compared to bulk organic carbon, about 3–6 ‰ for GS09-ROV7-2 and higher for the other samples (9–16 ‰). Lipids are generally recognized as lacking ^{13}C compared to bulk biomass (Hayes 2001), but this difference in offset points again to the distinct communities that inhabit the different locations. The $\delta^{13}C$ values of $C_{16:1\omega5c}$ fatty acids were about 2–4 ‰ lower than those of $C_{16:1\omega7c}$ fatty acids. The generally depleted $\delta^{13}C$ values of unsaturated fatty acids are in

the same range of values observed for SRB grown autotrophically (Londry et al. 2004). In one species of SRB (*D. acetoxidans*), the $\delta^{13}C$ values of $C_{16:1}$ and $C_{18:1}$ fatty acids varied significantly with the position of the double bond, an observation that was attributed to the selectivity of the enzyme introducing this double bond (Londry et al. 2004). In that case, the unsaturated fatty acids with the double bonds closer to the aliphatic end of the molecule were more depleted in ^{13}C in agreement with the signature that was observed here. The study by Londry et al. (2004) demonstrated that in certain microorganisms the biosynthesis of unsaturated fatty acids can lead to structurally related compounds having markedly different $\delta^{13}C$ signatures.

The isotope values reported for fatty acids indicative of SRB in methane seeps are frequently much more negative (less than −80 ‰) than those observed in our samples (Elvert et al. 2003). Methane, CO_2, and biomass can all be extremely depleted in ^{13}C in AOM environments (Alperin and Hoehler 2009). However, at Loki's Castle the bacteria may not be directly linked to AOM, although some members may use carbon sources originally derived from methane, such as DIC (CO_2 from methane oxidation) or recycled biomass (from methanotrophic organisms).

Conclusions

Our biomarker and isotope inventories of samples from the Loki's Castle low-temperature diffuse venting area reveal substantial differences in chimney formation and lipid composition of microbial consortia. Multiple sulfur isotope data from an inactive silica–barite chimney suggest that barite precipitated from ambient seawater sulfate. Minor admixture of oxidized sulfur species from hydrothermal fluids is suggested, but no evidence for microbial sulfate reduction is discernible. This is different from the active barite chimney, where barite precipitated from a fluid that was affected by microbial sulfate reduction in the sediment below. Our biomarker data indicate the presence of diverse consortia of archaea and bacteria in the hydrothermal sediment and chimneys, most likely involved in the effective cycling of sulfur species as well as oxidation of methane and ammonia. Bacteria seem to be the dominant microorganisms in the active and inactive chimney barite and in the sediment as indicated by abundant unsaturated and branched fatty acids. However, the predominance of archaeal GMGTs with up to four rings in the silica-rich interior of the extinct chimney indicates the presence of hyperthermophilic archaea in the chimney when it was still emanating hot fluids. These findings were unexpected, as temperatures in this area were generally thought to be much lower. This indicates the heterogeneity of flow patterns, temperatures, and chemistry of ascending fluids at this vent site. Further oxygen isotope analyses on purified silica fractions are needed to calculate a reliable formation temperature of the chimney and verify high temperatures as indicated by the presence of GMGTs. Moreover, lipid analysis and age determination of other extinct chimneys from this heterogeneous vent area will give information about the preservation potential of biomarker lipids and help interpret fossil microbial communities.

Acknowledgments We would like to thank the crew and Rolf Birger Pedersen (cruise leader) onboard the R/V *G.O. Sars* during the cruises in 2009 and 2010 for their assistance at sea. Tamara Baumberger and Ingunn Hindenes Thorseth are thanked for precious help with sampling. We would also like to thank an anonymous reviewer for constructive comments that considerably improved the quality of the manuscript. This work was supported by the Swiss National Science Foundation (SNF projects 20MA21-115916 and 200020-132804) and by the EuroMARC programme of the European Science Foundation (ESF) through the 'H_2DEEP—Ultraslow spreading and hydrogen based deep biosphere' project.

References

Alperin MJ, Hoehler TM (2009) Anaerobic methane oxidation by archaea/slufate reducing bacteria aggregates: 2 Isotopic constraints. Am J Sci 309:958–984

Amend JP, Shock EL (2001) Energetics of overall metabolic reactions of thermophilic and hyperthermophilic Archaea and Bacteria. FEMS Microbiol Rev 25:175–243

Baumberger T (2011) Volatiles in marine hydrothermal systems. PhD thesis, ETH Zurich, Switzerland (http://dx.doi.org/10.3929/ethz-a-007230100)

Bian L, Hinrichs KU, Xie T, Brassell SC, Iversen N, Fossing H, Jørgensen BB, Hayes JM (2001) Algal and archaeal polyisoprenoids in a recent marine sediment: Molecular isotopic evidence for anaerobic oxidation of methane. Geochim Geophys Geosys 2. doi: 10.1029/2000GC000112

Blöchl E, Burggraf S, Fiala G, Laurerer G, Huber G, Huber R, Rachel R, Segerer A, Stetter KO, Volkl B (1995) Isolation, taxonomy and phylogeny of hyperthermophilic microorganisms. World J Microbiol Biotechnol 11:9–16

Blumenberg M, Seifert R, Reitner J, Pape T, Michaelis W (2004) Membrane lipid patterns typify distinct anaerobic methanotrophic consortia. Proc Nat Acad Sci 101:11111–11116

Blumenberg M, Seifert R, Petersen S, Michaelis W (2007) Biosignatures present in a hydrothermal massive sulfide from the Mid-Atlantic Ridge. Geobiology 5:435–450

Blumenberg M, Seifert R, Buschmann B, Kiel S, Thiel V (2012) Biomarkers reveal diverse microbial communities in black smoker sulfides from Turtle Pits (Mid-Atlantic Ridge, Recent) and Yaman Kasy (Russia, Silurian). Geomicrobiol J 29:66–75

Boyd ES, Pearson A, Pi YD, Li WJ, Zhang YG, He L, Zhang CL, Geesey GG (2011) Temperature and pH controls on glycerol dibiphytanyl glycerol tetraether lipid composition in the hyperthermophilic crenarchaeon *Acidilobus sulfurireducens*. Extremophiles 15:59–65

Burgess EA, Unrine JM, Mills GL, Romanek CS, Wiegel J (2012) Comparative geochemical and microbiological characterization of two thermal pools in the Uzon Caldera, Kamchatka, Russia. Microbial Ecol 63:471–489

Canfield DE, Raiswell R (1999) Evolution of the sulfur cycle. Am J Sci 299:7–9

Corliss JB, Dymond J, Gordon LI, Edmond JM, Herzen RPV, Ballard RD, Green K, Williams D, Bainbridge A, Crane K, Vanandel TH (1979) Submarine thermal springs on the Galapagos Rift. Science 203:1073–1083

De la Torre JR, Walker CB, Ingalls AE, Konneke M, Stahl DA (2008) Cultivation of a thermophilic ammonia oxidizing archaeon synthesizing crenarchaeol. Environ Microbiol 10:810–818

Dowling NJE, Widdel F, White DC (1986) Phospholipid ester-linked fatty-acid biomarkers of acetate-oxidizing sulfate-reducers and other sulfide-forming bacteria. J Gen Microbiol 132: 1815–1825

Eickmann B, Thorseth IH, Peters M, Strauss H, Bröcker M, Pedersen RB (2014) Barite in hydrothermal environments as a recorder of sub-seafloor processes: A multiple isotope study from the Loki's Castle vent field. Geobiology

Elvert M, Suess E, Whiticar MJ (1999) Anaerobic methane oxidation associated with marine gas hydrates: superlight C-isotopes from saturated and unsaturated C_{20} and C_{25} irregular isoprenoids. Naturwissenschaften 86:295–300

Elvert M, Boetius A, Knittel K, Jørgensen BB (2003) Characterization of specific membrane fatty acids as chemotaxonomic markers for sulfate-reducing bacteria involved in anaerobic oxidation of methane. Geomicrobiol J 20:403–419

Elvert M, Hopmans EC, Treude T, Boetius A, Suess E (2005) Spatial variations of methanotrophic consortia in cold methane seeps: implications from a high-resolution molecular and isotopic approach. Geobiology 3:195–209

Gibson RA, van der Meer MTJ, Hopmans EC, Reysenbach AL, Schouten S, Sinninghe Damsté JS (2013) Comparison of intact polar lipid with microbial community composition of vent deposits of the Rainbow and Lucky Strike hydrothermal fields. Geobiology 11:72–85

Guezennec J, Ortega-Morales O, Raguenes G, Geesey G (1998) Bacterial colonization of artificial substrate in the vicinity of deep-sea hydrothermal vents. FEMS Microbiol Ecol 26:89–99

Hannington MD, Scott SD (1988) Mineralogy and geochemistry of a hydrothermal silica–sulfide–sulfate spire in the caldera of Axial Seamount, Juan de Fuca Ridge. Can Min 26:603–625

Hayes JM (2001) Fractionation of the isotopes of carbon and hydrogen in biosynthetic processes. In: Valley J, Cole D (eds) Stable isotope geochemistry 43. Mineral Soc Am, Washington

Herzig PM, Hannington MD (1995) Polymetallic massive sulfides at the modern seafloor a review. Ore Geol Rev 10:95–115

Herzig PM, Becker KP, Stoffers P, Bäcker H, Blum N (1988) Hydrothermal silica chimney fields in the Galapagos Spreading Center at 86° W. Earth Planet Sci Lett 89:261–272

Hopmans EC, Schouten S, Pancost RD, van der Meer MTJ, Sinninghe Damsté JS (2000) Analysis of intact tetraether lipids in archaeal cell material and sediments by high performance liquid chromatography/atmospheric pressure chemical ionization mass spectrometry. Rap Comm Mass Spectrom 14:585–589

Hopmans EC, Weijers JWH, E Schefuß, Herford L, Schouten S, Sinninghe Damsté JS (2004) A novel proxy for terrestrial organic matter in sediments based on branched and isoprenoid tetraether lipids. Earth Planet Sci Lett 224:107–116

House CH, Schopf JW, Stetter KO (2003) Carbon isotopic fractionation by Archaeans and other thermophilic prokaryotes. Org Geochem 34:345–356

Hu J, Meyers PA, Chen G, Peng P, Qunhui Y (2012) Archaeal and bacterial glycerol dialkyl glycerol tetraethers in sediments from the Eastern Lau Spreading Center, South Pacific Ocean. Org Geochem 43:162–167

Jaeschke A, Jorgensen SL, Bernasconi SM, Pedersen RB, Thorseth IH, Früh-Green GL (2012) Microbial diversity of Loki's Castle black smokers at the Arctic Mid-Ocean Ridge. Geobiology. doi:10.1111/gbi.12009

Janecky DR, Seyfried WE (1984) Formation of massive sulfide deposits on oceanic ridge crests—incremental reaction models for mixing between hydrothermal solutions and seawater. Geochim Cosmochim Acta 48:2723–2738

Kashefi K, Lovley DR (2003) Extending the upper temperature limit for life. Science 301:934

Kato S, Takano Y, Kakegawa T, Oba H, Inoue K, Kobayashi C, Utsumi M, Marumo K, Kobayashi K, Ito Y, Ishibashi JI, Yamagishi A (2010) Biogeography and biodiversity in sulfide structures of active and inactive vents at deep-sea hydrothermal fields of the Southern Mariana Trough. Appl Environ Microbiol 76:2968–2979

Kellermann MY, Wegener G, Elvert M, Yoshinaga MY, Lin YS, Holler T, Mollar XP, Knittel K, Hinrichs KU (2012) Autotrophy as a predominant mode of carbon fixation in anaerobic methane-oxidizing microbial communities. Proc Nat Soc Am 109:19321–19326

Kelly DS, Baross JA, Delaney JR (2002) Volcanoes, fluids, and life at mid-ocean ridge spreading centers. Annu Rev Earth Planet Sci 30:385–491

Kletzin A, Urich A, Müller F, Bandeiras TM, Gomes CM (2004) Dissimilatory oxidation and reduction of elemental sulfur in thermophilic archaea. J Bioenerg Biomembr 36:77–91

Knappy CS, Chong JPJ, Keely BJ (2009) Rapid discrimination of archaeal tetraether lipid cores by liquid chromatography–tandem mass spectrometry. J Amer Soc Mass Spec 20:51–59

Knappy CS, Nunn CEM, Morgan HW, Keely BJ (2011) The major lipid cores of the archaeon *Ignisphaera aggregans*: implications for the phylogeny and biosynthesis of glycerol monoalkyl glycerol tetraether isoprenoid lipids. Extremophiles 15:517–528

Koga Nakano M (2008) A dendrogram of archaea based on lipid component parts composition and its relationship to rRNA phylogeny. Sys Appl Microbiol 31:169–182

Koga Y, Morii H (2005) Recent advances in structural research on ether lipids from archaea including comparative and physiological aspects. Biosci Biotech Biochem 69:2019–2034

Kongsrud JA, Rapp HT (2012) *Nicomache (Loxochona) lokii* sp.nov. (Annelida: Polychaeta: Maldanidae) from the Loki's Castle vent field: an important structure builder in an Arctic vent system. Polar Biol 35:161–170

Kormas KA, Tivey MK, Von Damm K, Teske A (2006) Bacterial and archaeal phylotypes associated with distinct mineralogical layers of a white smoker spire from a deep-sea hydrothermal vent site (9°N, East Pacific Rise). Environ Microbiol 8:909–920

Lai D, Springstead JR, Monbouquette HG (2008) Effect of growth temperature on ether lipid biochemistry in *Archaeoglobus fulgidus*. Extremophiles 12:271–278

Lilley MD, Butterfield DA, Olson EJ, Lupton JE, Macko SA, Mcduff RE (1993) Anomalous CH4 and NH4+ concentrations at an unsedimented mid-ocean-ridge hydrothermal system. Nature 364:45–47

Lincoln SA, Bradley AS, Newman SA, Summons RE (2013) Archaeal and bacterial glycerol dialkyl glycerol tetraether lipids in chimneys of the Lost City Hydrothermal Field. Org Geochem 60:45–53

Londry KL, Jahnke LL, Des Marais DJ (2004) Stable carbon isotope ratios of lipid biomarkers of sulfate reducing bacteria. Appl Environ Microbiol 70:745–751

Londry KL, Dawson KG, Grover HD, Summons RE, Bradley AS (2008) Stable carbon isotope fractionation between substrates and products of *Methanosarcina barkeri*. Org Geochem 39:608–621

Lopez-Garcia P, Duperron S, Philippot P, Foriel J, Susini J, Moreira D (2003) Bacterial diversity in hydrothermal sediment and epsilonbacterial dominance in experimental microcolonizers at the Mid-Atlantic Ridge. Environ Microbiol 5:961–976

McCollom TM, Shock EL (1997) Geochemical constraints on chemolithoautotrophic metabolism by microorganisms in seafloor hydrothermal systems. Geochim Cosmochim Acta 61:4375–4391

Miroshnichenko ML (2004) Thermophilic microbial communities of deep-sea hydrothermal vents. Microbiology 73:1–13

Morii H, Eguchi T, Nishihara M, Kakinuma K, Konig H, Koga Y (1998) A novel ether core lipid with H-shaped C-80-isoprenoid hydrocarbon chain from the hyperthermophilic methanogen *Methanothermus fervidus*. Biochim Biophys Acta 1390:339–345

Noguchi T, Shinjo R, Ito M, Takada J, Oomori T (2011) Barite geochemistry from hydrothermal chimneys of the Okinawa Trough: insight into chimney formation and fluid/sediment interaction. J Mineral Petrol Sci 106:26–35

Ono S, Wing B, Johnston DT, Farquhar J, Rumble D (2006) Mass-dependent fractionation of quadrupole stable sulfur isotope system as a new tracer of sulfur biogeochemical cycles. Geochim Cosmochim Acta 70:2238–2252

Ono S, Shanks WC III, Rouxel OJ, Rumble D (2007) S-33 constraints on the seawater sulfate contribution in modern seafloor hydrothermal vent sulfides. Geochim Cosmochim Acta 71:1170–1182

Ono S, Keller N, Rouxel O, Alt JC (2012) Sulfur-33 constraints on the origin of secondary pyrite in altered oceanic basement. Geochim Cosmochim Acta 87:323–340

Pancost RD, Sinninghe Damsté JS, De Lint S, Van Der Maarel MJEC, Gottschal JC (2000) Biomarker evidence for widespread anaerobic methane oxidation in Mediterranean sediments by a consortium of methanogenic archaea and bacteria. Appl Environ Microbiol 66:1126–1132

Paytan A, Mearon S, Cobb K, Kastner M (2002) Origin of marine barite deposits: Sr and S isotope characterization. Geology 30:747–750

Pearson A, Huang Z, Ingalls AE, Romanek CS, Wiegel J, Freeman KH, Smittenberg RH, Zhang CL (2004) Nonmarine crenarchaeol in Nevada hot springs. Appl Environ Microbiol 70:5229–5237

Pedersen RB, Rapp HT, Thorseth IH, Lilley MD, Barriga FJAS, Baumberger T, Flesland K, Fonseca R, Fruh-Green GL, Jorgensen SL (2010) Discovery of a black smoker vent field and vent fauna at the Arctic Mid-Ocean Ridge. Nature Communications 1

Pitcher A, Rychlik N, Hopmans EC, Spieck E, Rijpstra WIC, Ossebar J, Schouten S, Wagner M, Sinninghe Damsté JS (2010) Crenarchaeol dominates the membrane lipids of "Candidatus *Nitrososphaera gargensis*", a thermophilic Group I.1b Archaeon. ISME J 4:542–552

Reysenbach AL, Cady SL (2001) Microbiology of ancient and modern hydrothermal systems. Trends Microbiol 9:79–86

Risatti JB, Rowland SJ, Yon DA, Maxwell JR (1984) Stereochemical studies of acyclic isoprenoids-XI. Lipids of methanogenic bacteria and possible contributions to sediments. Org Geochem 6:93–114

Schlitzer R (2013) Ocean Data View. http://odv.awi.de

Schönheit K, Schäfer T (1995) Metabolism of hyperthermophiles. World J Microbiol Biotechnol 11:26–57

Schouten S, Hopmans EC, Schefuss E, Sinninghe Damsté JS (2002) Distributional variations in marine crenarchaeotal membrane lipids: a new tool for reconstructing ancient sea water temperatures? Earth Planet Sci Lett 204:265–274

Schouten S, Wakeham SG, Hopmans EC, Sinninghe Damsté JS (2003) Biogeochemical evidence that thermophilic archaea mediate the anaerobic oxidation of methane. Appl Environ Microbiol 69:1680–1686

Schouten S, van der Meer MTJ, Hopmans EC, Rijpstra WIC, Reysenbach AL, Ward DM, Sinninghe Damsté JS (2007) Archaeal and bacterial glycerol dialkyl glycerol tetraether lipids in hot springs of Yellowstone National Park. Appl Environ Microbiol 73:6181–6191

Schouten S, Baas M, Hopmans EC, Reysenbach AL, Sinninghe Damsté JS (2008a) Tetraether membrane lipids of Candidatus "*Aciduliprofundum boonei*", a cultivated obligate thermoacidophilic euryarchaeote from deep-sea hydrothermal vents. Extremophiles 12:119–124

Schouten S, Baas M, Hopmans EC, Sinninghe Damsté JS (2008b) An unusual isoprenoid teraether lipid in marine and lacustrine sediments. Org Geochem 39:1033–1038

Schouten S, Hopmans EC, Sinninghe Damsté JS (2013) The organic geochemistry of glycerol dialkyl glycerol tetraether lipids. Org Geochem 54:19–61

Schrenk MO, Kelley DS, Delaney JR, Baross JA (2003) Incidence and diversity of microorganisms within the walls of an active deep-sea sulfide chimney. Appl Environ Microbiol 69:3580–3592

Shanks WCP, Morgan LA, Balistrieri L, Alt JC (2007) Hydrothermal fluids, siliceous hydrothermal deposits, and hydrothermally altered sediments in Yellowstone Lake. USGS publication

Sinninghe Damsté JS, Rijpstra WIC, Hopmans EC, Weijers JWH, Foesel BU, Overmann J, Dedysh SN (2011) 13,16-dimethyl octacosanedioic acid (iso-diabolic acid), a common membrane-spanning lipid of *Acidobacteria* Subdivisions 1 and 3. Appl Environ Microbiol 77:4147–4154

Steen IH, Thorseth IH, Roalkvam I, Dahle H, Stokke R, Pedersen RB (2011) Structure and function of microbial communities associated with low-temperature hydrothermal venting and formation of barite chimneys at Loki's Castle vent field. Abstract. In: Goldschmidt conference, Florence, Italy

Stetter KO, Gaag G (1983) Reduction of molecular sulfur by methanogenic bacteria. Nature 305:309–311

Sugai A, Uda I, Itoh YH, Itoh T (2004) The core lipid composition of the 17 strains of hyperthermophilic archaea, Thermococcales. J Oleo Sci 53:41–44

Suzuki Y, Inagaki F, Takai K, Nealson KH, Horikoshi K (2004) Microbial diversity in inactive chimney structures from deep-sea hydrothermal systems. Microbial Ecol 47:186–196

Takai K, Komatsu T, Inagaki F, Horikoshi K (2001) Distribution of archaea in a black smoker chimney structure. Appl Environ Microbiol 67:3618–3629

Thiel V, Peckmann J, Seifert R, Wehrung P, Reitner J, Michaelis W (1999) Highly isotopically depleted isoprenoids: molecular markers for ancient methane venting. Geochim Cosmochim Acta 63:3959–3966

Thode HG, Monster J, Dunford HB (1961) Sulphur isotope geochemistry. Geochim Cosmochim Acta 25:159–174

Tivey MK (1995) The influence of hydrothermal fluid composition and advection rates on black smoker chimney mineralogy—insights from modeling transport and reaction. Geochim Cosmochim Acta 59:1933–1949

Torres ME, Bohrmann G, Dubé TE, Poole FG (2003) Formation of modern and Paleozoic stratiform barite at cold methane seeps on continental margins. Geology 31:897–900

Uda I, Sugai A, Itoh YH, Itoh T (2001) Variation in molecular species of polar lipids from *Thermoplasma acidophilum* depends on growth temperature. Lipids 36:103–105

Uda I, Sugai A, Itoh YH, Itoh T (2004) Variation in molecular species of core lipids from the order Thermoplasmatales strains depend on growth temperature. J Oleo Sci 53:399–404

Urabe T, Kusakabe M (1990) Barite silica chimneys from the Sumisu Rift, Izu-Bonin Arc: possible analog to hematitic chert associated with Kuroko deposits. Earth Planet Sci Lett 100:283–290

van de Vossenberg JLCM, Driessen AJM, Konings WN (1998) The essence of being extremophilic: the role of the unique archaeal membrane lipids. Extremophiles 2:163–170

Weijers JWH, Schouten S, van den Donker JC, Hopmans EC, Sinninghe Damsté JS (2007) Environmental controls on bacterial

tetraether membrane lipid distribution in soils. Geochim Cosmochim Acta 71:703–713

Zhang CL, Huang ZY, Cantu J, Pancost RD, Brigmon RL, Lyons TW, Sassen R (2005) Lipid biomarkers and carbon isotope signatures of a microbial (Beggiatoa) mat associated with gas hydrates in the Gulf of Mexico. Appl Environ Microbiol 71:2106–2112

Zhang CL, Pearson A, Li YL, Mills G, Wiegel J (2006) Thermophilic temperature optimum for crenarchaeol synthesis and its implication for archaeal evolution. Appl Environ Microbiol 72:4419–4422